FULL ARTICLE

Instant polarized light microscopy for imaging collagen microarchitecture and dynamics

Bin Yang[1,2] | Po-Yi Lee[1,3] | Yi Hua[1] | Bryn Brazile[1] | Susannah Waxman[1] | Fengting Ji[1,3] | Ziyi Zhu[1,3] | Ian A. Sigal[1,3]*

[1]Department of Ophthalmology, University of Pittsburgh School of Medicine, Pittsburgh, Pennsylvania

[2]Department of Engineering, Rangos School of Health Sciences, Duquesne University, Pittsburgh, Pennsylvania

[3]Department of Bioengineering, Swanson School of Engineering, University of Pittsburgh, Pittsburgh, Pennsylvania

*Correspondence
Ian A. Sigal, Ocular Biomechanics Laboratory, Department of Ophthalmology, University of Pittsburgh School of Medicine, 203 Lothrop Street, Rm 930, Pittsburgh PA, 15213, USA.
Email: ian@ocularbiomechanics.com,
www.ocularbiomechanics.com

Abstract

Collagen fibers are a primary load-bearing component of connective tissues and are therefore central to tissue biomechanics and pathophysiology. Understanding collagen architecture and behavior under dynamic loading requires a quantitative imaging technique with simultaneously high spatial and temporal resolutions. Suitable techniques are thus rare and often inaccessible. In this study, we present instant polarized light microscopy (IPOL), in which a single snapshot image encodes information on fiber orientation and retardance, thus fulfilling the requirement. We utilized both simulation and experimental data from collagenous tissues of chicken tendon, sheep eye, and porcine heart to evaluate the effectiveness of IPOL as a quantitative imaging technique. We demonstrate that IPOL allows quantitative characterization of micron-scale collagen fiber architecture at full camera frame rates (156 frames/second herein).

KEYWORDS

biomechanics, collagen, deformation, polarized light microscopy
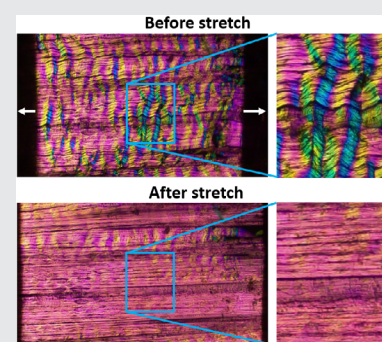
1 | INTRODUCTION

Collagen fiber organization varies through our bodies, from highly anisotropic in tendon [1], to isotropic in skin [2, 3] and parts of sclera [4, 5]. This organization strongly influences the mechanical properties and behavior of tissues and organs [2]. To fully understand organ physiology and pathology, it is essential to understand collagen fiber organization [6, 7]. One of the techniques most often deployed to visualize and characterize collagen organization and architecture is polarized light microscopy (PLM) [8–10]. PLM takes advantage of the intrinsic birefringence of collagen, and does not require tissue labels or stains. Conventional quantitative analysis of collagen organization using PLM, however, requires multiple images, typically four, under various polarization states [8, 11–13]. This slows down image acquisition and requires image registration that may decrease image quality. Hence, PLM works well when imaging tissues under static [14, 15] or quasi-static conditions [1, 16], but not when the tissues are under dynamic loading.

Several methods have been proposed to improve the speed of PLM imaging [12, 17–19]. One approach is to switch polarization states quickly [17, 18]. Another approach is to capture all four images simultaneously using pixel multiplexing on a single image sensor [12, 20].

Although excellent biomechanics information has been obtained using these techniques [21, 22], the improved imaging speed comes at the cost of spatial resolution. In addition, these techniques need post-processing to derive the information of interest, such as fiber orientation and local retardance. This makes real-time visualization more challenging, and requires previewing analysis output on a computer screen, rather than seeing objects directly through the microscope. Shribak recently introduced a variation of PLM based on a single image, which does not require post-processing to reveal variations in collagen orientation or retardance [23]. Shribak, however, only presented the technique qualitatively. Our goal in this work was to demonstrate a technique inspired by Shribak's original work, which we termed instant polarized light microscopy (IPOL). The analysis techniques we introduce show that IPOL is suitable for the quantitative analysis of the architecture and dynamics of collagenous tissues with high spatial and temporal resolutions. The robustness of IPOL was demonstrated for sheep eyes, pig chordae tendineae, and chicken tendon.

2 | METHODS

This section is organized into four parts. In section 2.1, we describe the IPOL imaging system we developed based on a commercial inverted microscope. As we will show, images acquired using IPOL encode information on fiber orientation and retardance through pixel color and intensity. In section 2.2, we introduce a framework based on Mueller-matrix formalism to determine the relationship between color and fiber orientation over a wide range of tissue retardance values suitable for many imaging systems. This framework is evaluated and verified using simulation. With the general color-angle mapping method, in section 2.3 we demonstrate experimentally the quantitative color-angle mapping. Specifically, we use chicken leg tendon tissues at known orientations to determine the system-specific color-angle mapping. Finally, in section 2.4, we demonstrate IPOL applied to image and quantify collagen architecture and dynamics of ocular, vascular, and musculoskeletal collagenous tissues.

2.1 | IPOL imaging system

We developed an IPOL imaging system on an inverted microscope (Olympus IX 83, Olympus, Tokyo, Japan) by retrofitting a polarization encoder in the illumination path and a polarization decoder in the imaging path, shown in Figure 1A. The schematic diagram of IPOL imaging system is shown in Figure 1B. Each polarizer group consisted of a linear polarizer and a z-cut quartz plate. Linear polarizers in the polarization encoder and
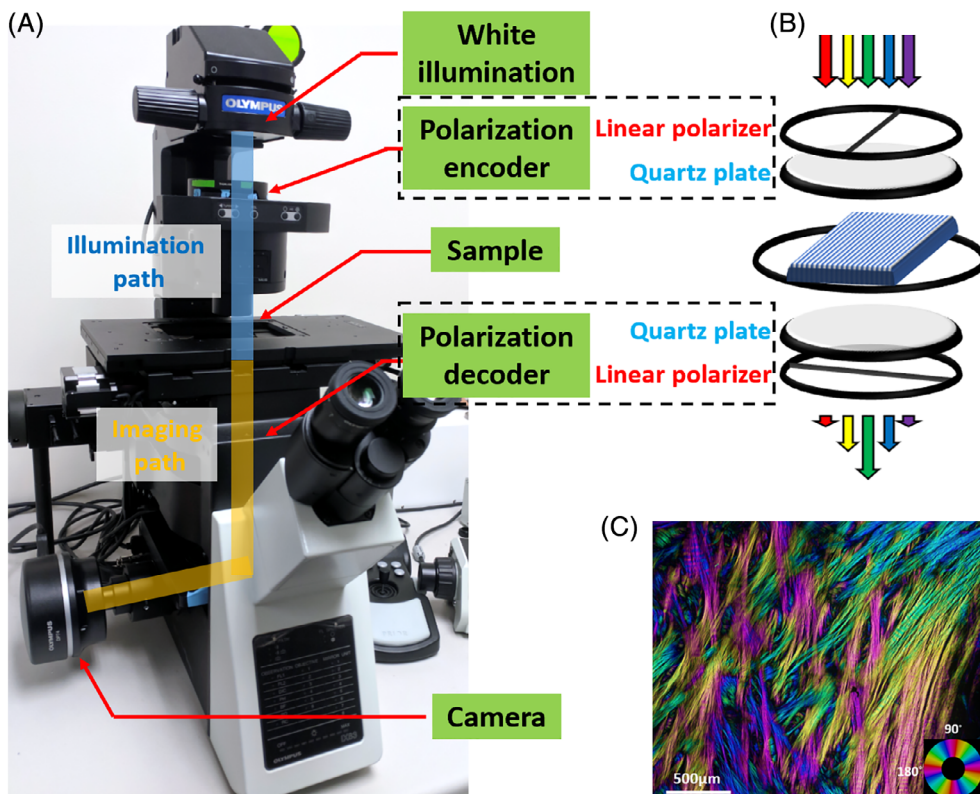
FIGURE 1 A, Instant polarized light microscopy (IPOL) imaging configuration on an inverted microscope. Polarization encoder and decoder are fitted into the illumination path and imaging path, respectively. Each polarizer group consists of a linear polarizer and a z-cut quartz plate. B, Schematic diagram of IPOL imaging system. Spectral distribution changes dependent on local fiber orientation. C, An example IPOL image showing interweaving collagen fibers in the posterior sclera of a sheep eye. Colors represent local fiber orientation

decoder were oriented orthogonally. A broadband white LED light source (IX3-LJLEDC, Olympus, Tokyo, Japan) was used for illumination and strain-free objectives were used for imaging. True-color fiber orientation-encoded images were acquired by a high-speed CMOS camera (acA1920-155uc, Basler AG, Ahrensburg, Germany). In Figure 1C, we show an example of an IPOL image of interweaving collagen fibers [5, 24] in the posterior sclera of a sheep eye. Colors in the image represent local fiber orientations, and intensity variations correlate to local retardance.

2.2 | IPOL simulation

A simulation framework was developed based on Mueller matrix formalism [25] to model the optical interactions between polarized light and the birefringent sample. Such interaction, based on the imaging configuration shown in Figure 1B, can be described using following equation:

$$S_{\text{out}}(\lambda, \varphi, \delta) = M_{90} M_{\text{rot}}(-\theta(\lambda)) M_{\text{tissue}}(\varphi, \delta) M_{\text{rot}}(\theta(\lambda)) M_0 S_{\text{in}}(\lambda) \tag{1}$$

where M is the Mueller matrix and S is the Stokes vector. To match the experimental setup, the spectrum S(λ) of an LED white light source (IX3-LJLEDC, Olympus, Tokyo, Japan) was used in the simulation. The illumination passes through a linear polarizer M_0 orientated at 0 degree and becomes linearly polarized. The polarization of the linearly polarized broadband illumination then undergoes a wavelength-dependent rotation $\theta(\lambda)$ introduced by a z-cut quartz before reaching the tissue. The wavelength-dependent rotation $\theta(\lambda)$ was previously reported at multiple wavelengths in the visible range [26]. We fitted the data and calculated $\theta(\lambda)$ every 1 nm from 400 to 700 nm. The birefringent collagenous tissue was modeled as a phase retarder, M_{tissue}, with the slow axis orientation (collagen fiber orientation) ϕ varying from 0 to 90 degrees, and the retardance δ varying from 0.1 to 1.2 radians. After passing through the tissue, the light undergoes an opposite polarization-dependent rotation at the second z-cut quartz, and is then analyzed by a linear polarizer, M_{90}, oriented at 90 degrees. For a given fiber orientation and retardance, S_{out} was calculated for all wavelengths between 400 and 700 nm. This process generates an output spectrum over the same wavelength range. To generate the corresponding RGB (**R**ed, **G**reen, **B**lue) color of the spectrum, color matching functions were used first to convert the spectrum to a set of tristimulus values [27], X, Y and Z, which was further

converted to R, G, and B values. The process of converting a spectrum to an RGB color is an established technique in colorimetry [27, 28]. It is worth noting that rotating the illumination polarization is equivalent to rotating the sample.

To facilitate quantitative analysis, the simulated color was converted from RGB space to HSV (**H**ue, **S**aturation, **V**alue) space [27]. The terms 'value' and "intensity" are interchangeable. We opted to use 'intensity' for consistency. We established the relationships between the hue and fiber orientation, and between the intensity and retardance.

2.3 | Experimental calibration: RGB color to orientation angle mapping

The simulations in section 2.2 provide valuable insight into the general imaging capabilities of IPOL. However, characteristics of the imaging system that were not incorporated in the simulations may affect the accuracy of the fiber orientations determined from the color image. Hence, we performed an experimental calibration and developed a system-specific color-angle conversion map. A thin section of chicken leg tendon was chosen due to its overall consistent fiber orientation along the longitudinal direction [8, 29]. Details of the tissue section preparation are provided below in section 2.4.3. IPOL images were acquired with the chicken tendon section at several controlled angles relative to the longitudinal fiber direction, from 0° to 90°, every 2°. The individual images were then registered using the FIJI software [30]. A region-of-interest (ROI) on the tissue was manually selected on the stack, and the hue of the ROI was extracted following the method described in section 2.2. A color-angle conversion map was then computed by a circular interpolation of the measured hue and its corresponding orientation angle. The fiber orientation map for all images was then obtained by searching hue value over the color-angle conversion map for corresponding angles for all pixels.

2.4 | Soft tissue imaging

To demonstrate the high spatial and temporal resolution imaging capabilities of IPOL, we used samples from three soft tissues: sheep optic nerve head, pig heart chordae tendineae, and chicken leg tendon. We chose them because all three have been used to study the general and disease-specific biomechanics of collagenous tissues [31–33]. Tendons, because of the fairly uniform collagen organization, are often used to demonstrate the accuracy

of fiber orientation quantification of PLM [8]. Due to the similarity to human eyes, sheep eyes are used in ophthalmology to understand the biomechanical role of collagen fiber architecture, especially the optic nerve head region [34]. Chordae tendineae are primarily composed of collagen fibers, and play essential roles in regulating the opening and closing of heart valve leaflets [35].

2.4.1 | Sheep optic nerve head

Sheep eyes from a local abattoir were prepared as described in detail previously [8]. Briefly, sheep eyes were enucleated within 4 hours after death and formalin-fixed for 24 hours at 22 mm Hg of intraocular pressure. The optic nerve head region was isolated using an 11-mm-diameter trephine and cryosectioned into 16-μm-thick coronal sections. Sections were imaged with a ×10 strain-free objective. To visualize regions larger than the field of view we used mosaicking [8].

2.4.2 | Pig chordae tendineae

A pig heart was obtained from a local abattoir, and chordae tendineae were isolated with a razor blade. One piece of fresh chordae tendineae was mounted onto a custom uniaxial stretching device and stretched longitudinally with a strain rate of 0.4/s and simultaneously imaged with a ×2 strain-free objective at 156 frames/s. During the testing, sample was kept hydrated by applying PBS solution on the sample surface. Note that the experimental testing was intended to demonstrate the potential of the technique, and does not necessarily represent the in vivo conditions. Further, no preconditioning was applied.

2.4.3 | Chicken leg tendon

Chicken leg tendons were used in two parts of this project: for the color-angle mapping calibration described in section 2.3, and for demonstrating IPOL use during uniaxial mechanical testing. All samples were obtained from food-grade chicken legs purchased from a local grocery store and processed within 4 hours of acquisition. The preparation of the sample for each experiment was different.

Color-angle mapping
A chicken leg tendon was dissected and fixed with 10% formalin for 24 hours while under load to remove the

natural undulations of collagen fibers, or crimp [36]. Following fixation, tendons were embedded and cryosectioned longitudinally into 30-μm-thick sections.

Uniaxial mechanical testing
A chicken leg tendon was dissected, and without fixing, cryo-sectioned longitudinally into 30-μm-thick sections. Sections were washed multiple times with PBS. In the uniaxial testing, a section was mounted to a custom device for mechanical testing while imaged using IPOL [37]. The stretch was applied until failure (rupture) of the section was observed. The stretching process lasted about 3 seconds and was imaged at 156 frames/second with a 4x strain-free objective.

3 | RESULTS

3.1 | IPOL simulation

Figure 2 shows the spectrum of the illumination and the simulated spectra at three fiber orientations: 30°, 60°, and 90°. When converting from spectrum to color, different spectral profiles generate different colors. In other words, fiber orientations are directly encoded in colors. The simulated colors of IPOL imaging are shown in Figure 3. The RGB color map (Figure 3A) demonstrates that the color and intensity in IPOL imaging are related to the local fiber orientation and retardance. This trend can be better appreciated by decomposing RGB color to HSV color. In the hue map (Figure 3B), we noticed that the color was independent of the retardance, and solely determined by the fiber orientation. Hue varies monotonically with fiber orientation (Figure 3D). The monotonic relationship ensures unique mapping between the hue
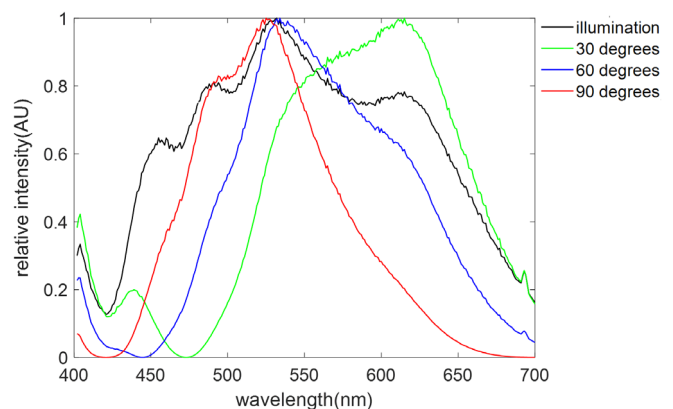
FIGURE 2 Spectrum of the illumination and simulated spectra at three fiber orientations. The relative intensity of spectra depends on the fiber orientation, which thus allows for color-angle mapping
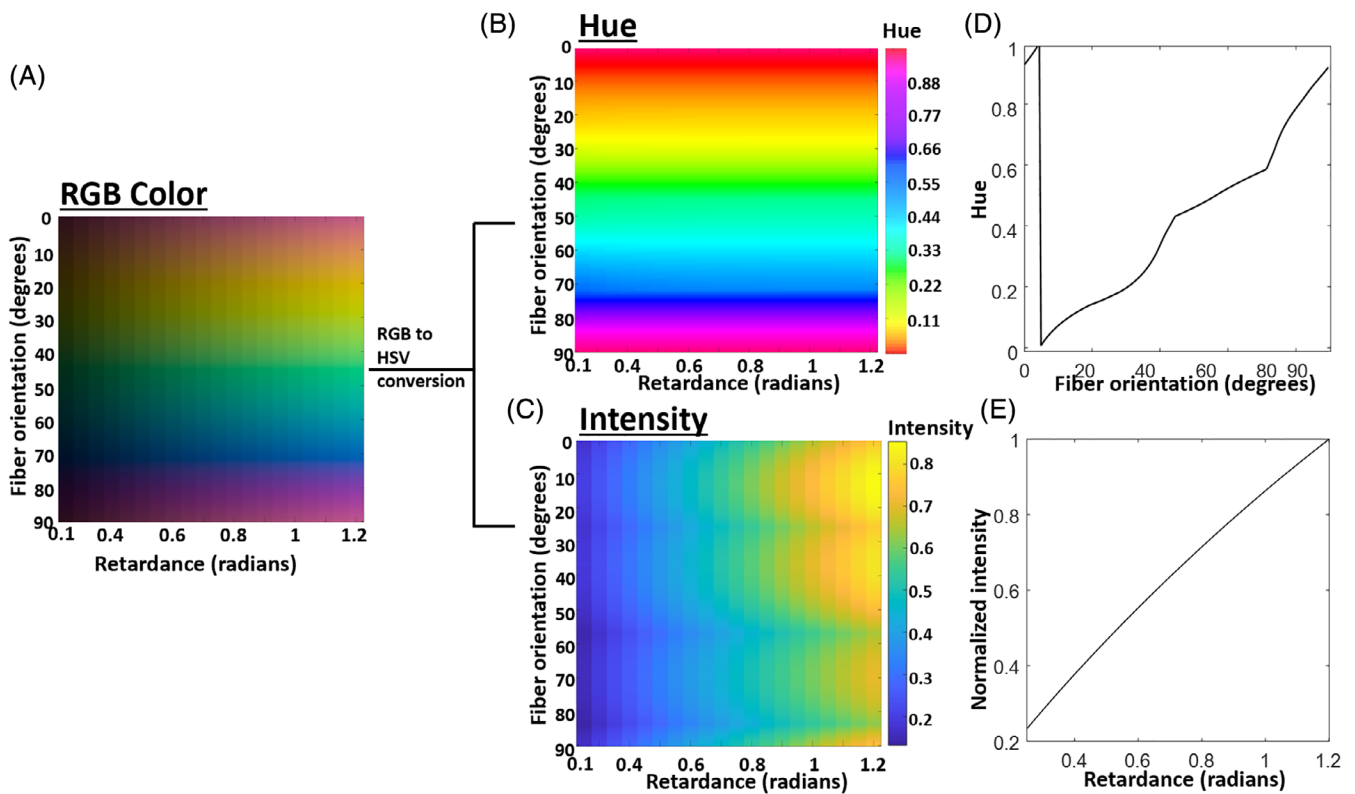
FIGURE 3   A, Simulated instant polarized light microscopy (IPOL) Red, Green, Blue (RGB) color maps covering fiber orientation angles from 0° to 90° and retardance from 0.1 to 1.2 radians. Corresponding, B, hue and, C, intensity maps obtained by converting the simulated RGB image to Hue, Saturation, Value (HSV) space. D, Monotonic and retardance-independent color-angle relationship obtained from the simulated hue map. E, At a set fiber orientation in the simulated intensity map, the intensity and retardance exhibit an approximately linear relationship
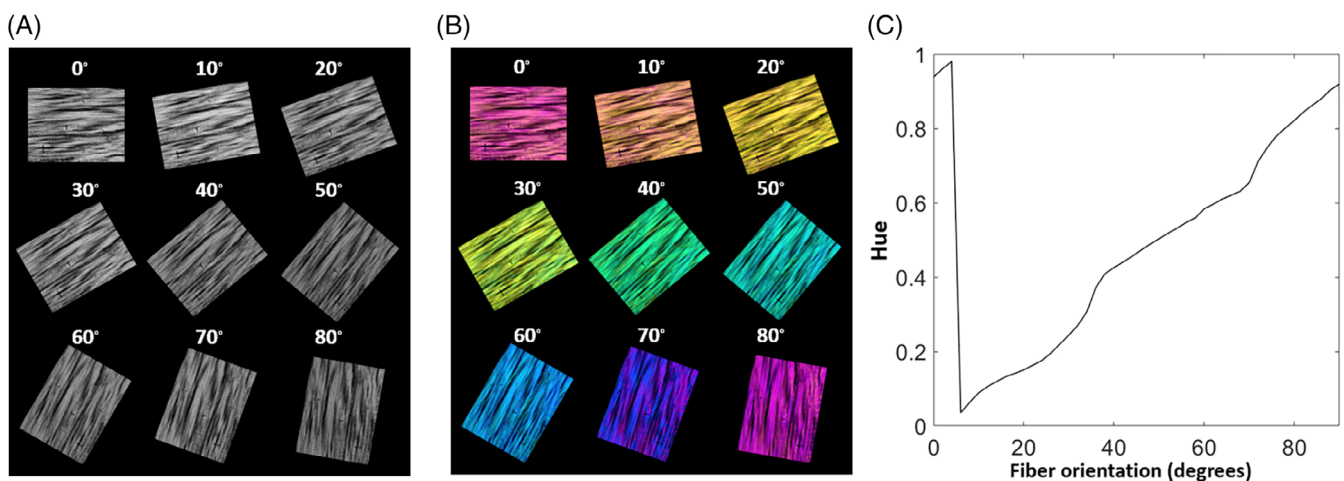
FIGURE 4   A, Intensity and B, instant polarized light microscopy (IPOL) images of chicken tendon sections. Colors correspond to fiber orientations. C, System-specific color-angle mapping. There is a monotonic relationship between the hue and fiber orientation, as predicted by the simulations shown in Figure 3D

and fiber orientation, which enables us to quantify the collagen fiber orientation from the color, accomplishing a primary goal of this study. Compared to the hue map, the intensity map exhibits a more complex dependency on the fiber orientation and retardance (Figure 3C). However, we noticed that at a given fiber orientation, the

normalized intensity was approximately linearly related to the retardance (Figure 3E). In our simulation study, we did not notice a role for saturation in the quantification.

3.2 | Experimental calibration: RGB color to orientation angle mapping

Images of a chicken tendon section were acquired at every 2° from 0° to 90°. We show a representative subset of images every 10° (Figure 4A). Images show that the color in IPOL (Figure 4B) is dependent on the fiber orientation. Although tendon is often considered to have fairly uniform collagen organization, IPOL clearly shows regional variations in fiber content and orientation. The averaged hue of a small region of the tendon section was calculated throughout the 45 images. The hue values were then interpolated and plotted against the fiber orientation as shown in Figure 4B. Notice the close similarity of the experimental calibration (Figure 4C) and the one based on simulations (Figure 3d).

3.3 | Soft tissue imaging

3.3.1 | Sheep optic nerve head

Example images of a sheep optic nerve head section (Figure 5) demonstrate the high-resolution potential of IPOL. Collagen fiber colors vary by their orientation, which significantly improves the visibility of different fiber families or bundles, and facilitates the visualization of various types of collagen architecture and interactions. The organization of the sclera into regions of circumferential, radial or isotropic fibers [38] is easily

discernible by IPOL (Figure 5A,B). At the center of the section is the scleral canal, with bright collagenous lamina cribrosa beams and vessel walls interspersed by neural tissues that are dark because of their low retardance. A close-up image (Figure 5C) reveals collagen crimp (red arrow) and collagen fiber interweaving (white arrow). The sub-bundle composition of a large fiber bundle can also be observed (cyan arrow) in Figure 5D. Note that due to the small field of view of the 10x objective, the image of the whole section was acquired using mosaicking.

3.3.2 | Pig chordae tendineae

With IPOL imaging, the pig chordae tendineae exhibited a layered architecture with a collagen core (purple color) surrounded by a cladding layer (green color) (Figure 6A), consistent with previous reports [39]. An intensity image of the pig chordae tendineae prior to stretching is show in Figure 6E. A total of 8.7% uniaxial stretch was applied to the chordae tendineae, and the deformation was recorded at 156 frames/second (Video S1). Figure 6A-D shows four stills of the stretching with an interval of 64 ms. During the first 192 ms, a strain of 7.68% was measured. The collagen core changed color from purple before stretch (Figure 6A) to blue after stretch (Figure 6D). Close inspection suggests collagen fiber uncrimping in the collagen core (Figure 6F), which was confirmed by plotting the fiber orientation along the chordae. A similar uncrimping process was also observed when manually pulling a piece of sheep sclera (Video S2). As shown in Figure 6G, collagen fiber orientation exhibits periodicity with fiber orientation alternating between 10° and 75°, indicating that collagen fibers were crimped before stretch. After the stretch, however,
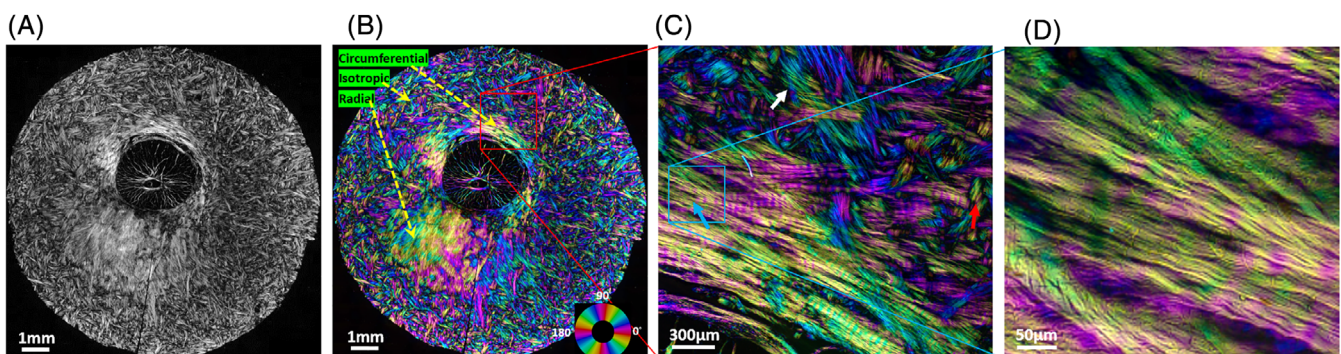
FIGURE 5 A, Intensity and B, instant polarized light microscopy (IPOL) image of a sheep optic nerve head section. Three major organizational components of the sclera are discernible. C, Close-up of peripapillary sclera revealed highly detailed collagen fiber features: two families of crossing fiber (white arrow), collagen fiber undulations or crimp (red arrow), and sub-bundle fiber composition (cyan arrow). D, Close-up of a bundle shows its fiber composition
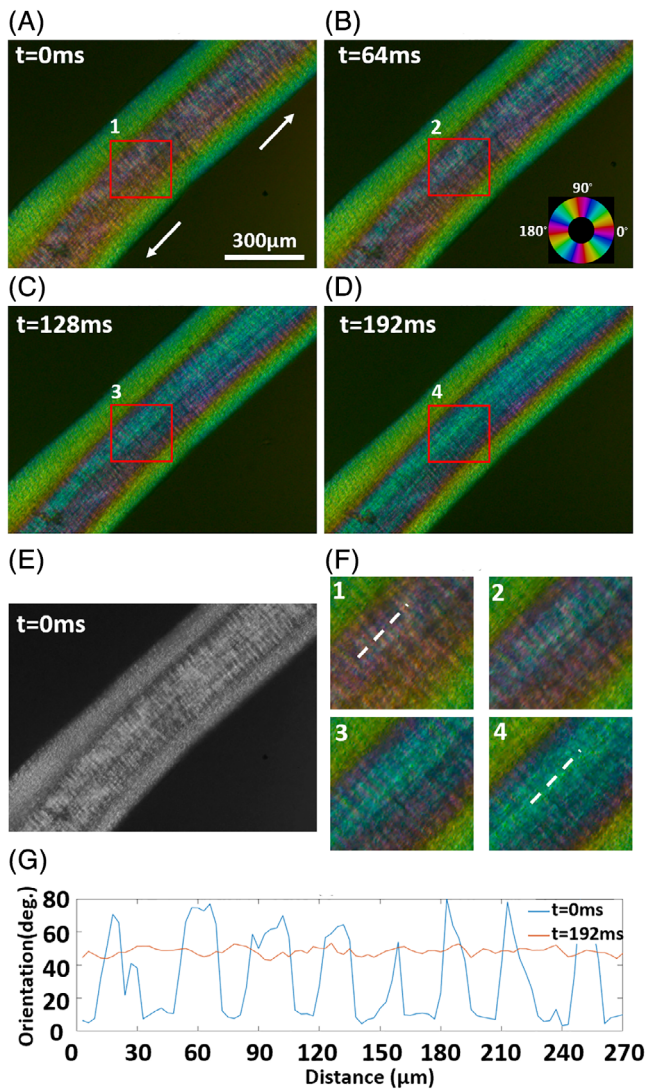
FIGURE 6 A-D, Instant polarized light microscopy (IPOL) images of a pig chordae tendineae under longitudinal stretch captured at four time points with an interval of 64 ms; white arrows indicate the stretching direction; E, Intensity image of the pig chordae tendineae at t = 0 ms. F, close-up of the core region (red square) showing color changes indicating uncrimping; G, fiber orientation profile along the white dashed line at t = 0 ms and t = 192 ms

the fiber orientation was overall flat with small variations around a mean orientation of 50°, aligned with the principal axis of the chordae. Interestingly, the cladding layer maintained the same green color throughout the stretching process, which may suggest that collagen fibers in the cladding layer underwent an extension process different from the core. It is worth noting that the thickness of the pig chordae tendineae is around 300 μm. Tissue scattering and shallow-depth-field of the objective prevent us from observing and tracking individual collagen fibers. Strong banding/crimp are discernible in Figure 6E indicative of complex 3D structure in chordae, which is

fully characterized by both in-plane and out-of-plane fiber orientation. The quantified fiber orientation should be considered as the representative orientation throughout the tissue thickness, and projected onto the imaging plane (in-plane fiber orientation). In fact, based on the intensity variation, it is may also be possible to quantify the out-of-plane fiber orientation.

3.3.3 | Chicken leg tendon

Collagen fibers in the chicken tendon are predominantly aligned with the tendon main axis. In the case of the section shown in Figure 7 this direction is horizontal. The orientation coloring of IPOL shows strong and relatively uniform crimp over the entire section (Figure 7A). Crimp is best visualized by re-coloring pixels in yellow/ purple (Figure 7E) based on the local orientation relative to its neighborhood average. The algorithm is described in detail elsewhere [40]. Upon applying a 16.7% uniaxial stretch, collagen fibers underwent uncrimping (Figure 7B,D,F) (Video S3). Figure 7I shows the deformation paths of collagen fibers in a small region (white box in Figure 7A) obtained using digital image correlation. Collagen fibers exhibit region-dependent deformation paths. As an illustration, we show collagen fiber uncrimping over a small region-of-interest (yellow box) at six time points from the acquired video (Figure 7G). High spatial and temporal resolutions of IPOL enabled the visualization of collagen fiber uncrimping with excellent details. For instance, we notice that collagen fibers in the lower part of the ROI uncrimping faster than those in the upper part. The biomechanical relevance of the uncrimping process can be understood by a force-stretch sketch (Figure 7H) (adapted from Reference [40]). Only minimal force is necessary to stretch a crimped fiber. As stretch increases, the fibers fully uncrimp and become "recruited." A recruited fiber requires a linearly increasing force to stretch further. A group of fibers thus exhibits a nonlinear increase in the force needed for stretch. The rate of collagen fiber uncrimping is directly related to the fiber recruitment, which determines tissue mechanical properties and responses under load. In addition to recruitment, there is inter-fiber sliding. Deformation tracking using image processing indicates that recruitment in tendon proceeds mostly through longitudinal stretch without substantial fiber rotations (Figure 7I).

4 | DISCUSSION

We have demonstrated that IPOL is well-suited for the imaging and quantitative study of the architecture and
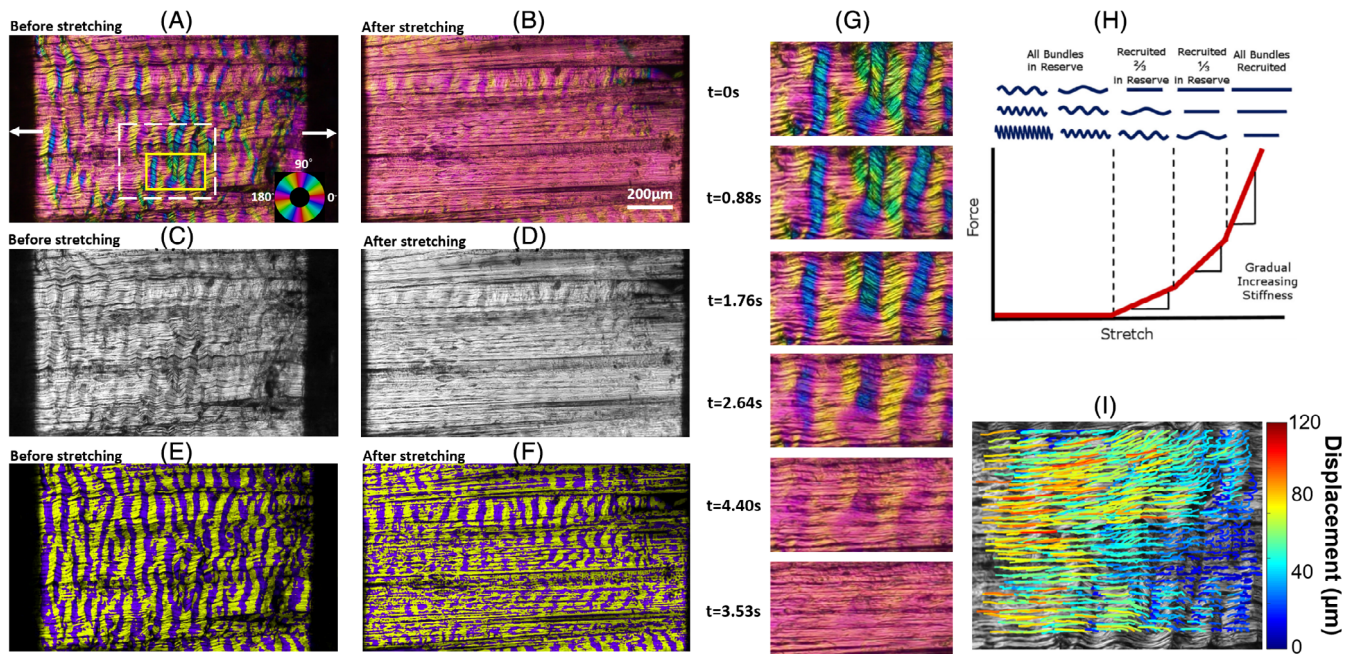
FIGURE 7   A,B, Instant polarized light microscopy (IPOL) image of a chicken tendon section before stretch and after stretch. Collagen fiber crimp can be identified by color changes along the fibers; white arrows indicate stretching direction. C,D, Intensity images of a chicken tendon section before stretch and after stretch. E,F, Crimp visualization before and after stretch. G, Time-sequence images of uncrimping process from a small region of the section (yellow box). H, Illustration of fiber recruitment under stretch (adapted from Reference [40]). I, Region-dependent deformation paths obtained from digital image correlation analysis shown overlaid on a greyscale image of the region (white box)

dynamics of complex collagenous tissues. Using a combination of experiments and simulations, we have shown how to establish a quantitative color-angle mapping technique through which fiber orientation can be accurately determined with excellent spatial and temporal resolution. The quantitative characterization of local orientation is useful by itself, as shown elsewhere in this paper. It is also important because it enables further visualization and analyses of essential micro-biomechanical processes, such as load-induced collagen fiber uncrimping. The detailed real-time images of collagen tissue dynamics demonstrate that IPOL imaging overcomes limitations on speed and/or resolution encountered with other techniques traditionally used to study soft tissue architecture and mechanics, such as second harmonic generated imaging [41], small angle light scattering [42] and conventional PLM imaging [8]. Together, the high spatial and temporal resolutions of IPOL enable a deeper insight into the relationship between tissue architecture and forces, and of their roles on tissue physiology and pathology, than is usually available with conventional techniques.

We highlight three important strengths of IPOL: (a) allows direct visualization of collagen architecture in color; (b) leverages the full spatial resolution of the microscope-camera system; (c) allows imaging of tissue dynamics and biomechanics with an acquisition speed

limited only by the camera. Below we expand on each of them, and on how their usefulness builds on each other to help improve understanding of tissue mechanics and dynamics.

Direct visualization in color

Collagen fibers in IPOL images are color-coded based on their local, pixel-scale, fiber orientation and retardance. In comparison to typical grayscale PLM images, this provides superior contrast, facilitating discernment of collagen fibers. Collagen fiber architecture, such as crimp and interweaving, become readily visible in color IPOL images which enables direct observation and discovery of novel tissue architecture and interactions while the tissue is being tested. Direct visualization of color at high frame rate is very convenient during general observation or when searching for "interesting tissue regions" as the orientation and retardance information are visible through the microscope ocular, even when the sample is moving and at different magnification levels. Techniques which require post-processing and calculations need time, and require users to see the results on a screen, rather than directly through the objective. This conceptually "distances" the sample from the measures.

Full spatial resolution

Conventional PLM typically requires multiple images to derive information such as fiber orientation [8, 43]. Acquiring multiple images requires time. As mentioned in the introduction, some have overcome this problem by switching polarization states quickly [17, 18]. Alternatively, it is possible to acquire the multiple images simultaneously using multiplexing on a single image sensor [12, 20]. Particularly powerful, and elegant, is the use of an analyzer grid directly built into the imaging sensor [21, 22]. However, multiple images have to be registered, which takes time and may introduce errors. Most importantly, registration usually involves interpolation, which reduces the spatial detail of the image. Multiplexing techniques, thus, involve some loss of resolution. IPOL, in contrast, preserves the highest spatial resolution offered by an imaging system by requiring only one image in order to visualize all fiber orientations, without the need for post-processing. When applied to complex biological tissues, this may reveal important architectural detail, such as sub-bundle fiber composition and crimp. For large samples, mosaicking can be used to achieve both large field-of-view and high resolution. Although mosaicking is not suitable for imaging tissue dynamics, it is still much faster than conventional PLM for imaging static samples, and preserves the camera's native resolution. It is worth noting that tissue complexity and homogeneity/inhomogeneity may affect the resolution of IPOL. If tissues are unstretched but highly organized, like crimp, IPOL can still produce images with high spatial and angular resolution. However, if tissues are disorganized or inhomogeneous through the thickness, IPOL will only show colors of representative local fiber orientations. Consequently, both spatial and angular resolution will be limited.

Camera-limited temporal resolution

Due to the imaging speed limitations, conventional PLM can only be employed in quasi-static tissue mechanical testing. In quasi-static testing, the dynamic process is split into multiple static steps. Images are taken at each step, registered and stacked to approximate the dynamic process. This method is acceptable when the loading speed is low, or when the tissue response is slow. However, when the loading speed is high (eg, blast and impact loading), this method would be problematic. Given adequate illumination, the imaging speed of IPOL is essentially only limited by the speed of the camera, which makes IPOL particularly well suited for imaging tissues under high-speed loading. High-speed imaging is particularly useful to study continuous yet complex tissue deformations under load, such as tissue viscoelasticity. Viscoelastic deformations at high speed are not the same as those at low speed [2]. IPOL captures complete and smooth tissue deformation trajectory in high spatiotemporal resolution, which allows us to study collagen fiber interactions at both tissue and fiber levels with unprecedented details.

We have shown a quantitative mapping of the colors in an IPOL image to collagen orientations. This mapping, however, is specific to our system. When developing future color-angle mappings for other systems, it is essential to consider the following factors: First, broad-band so-called white light sources may have substantially different spectral compositions. Second, microscope systems may introduce certain spectral attenuations through the optics, which would affect the detected colors. Finally, the tissues may vary in their absorption profile, for example due to pigments. All of the above could affect the colors observed in IPOL, and in turn the mappings. Thus, it is essential to establish a new color-angle mapping through a calibration process if the quantification condition is changed. It is worth noting that once the calibration is done, changing the acquisition settings of a microscope, such as exposure time, does not affect the quantification accuracy.

When analyzing IPOL data, it is important to consider that the orientation-encoded colors in IPOL are cyclic, that is, repeating every 90°. This helps discern even small differences in fiber orientation, allowing accurate measurement of collagen crimp, even when under high load. However, it also has some disadvantages: two fibers oriented perpendicular to each other have the same quantified orientation angles, exhibiting the same color. To adjudicate whether a 90-degree should be added to the quantified angle, the IPOL-angle could be supplemented using fiber orientations from gradient or Fourier analysis of the retardance map [44]. Such techniques are substantially less sensitive than IPOL, but are likely sufficient to discern orientation quadrant. Gradient and Fourier methods also do not provide information on tissue retardance.

A limitation of IPOL, as presented in this work, is that it is based on transmitted light microscopy. This, in turn, requires that the tissue samples are cut into fairly thin sections to be compatible with the configuration of a microscope, such as the magnification and numeric aperture, to achieve optimal imaging results. A thicker section may still be imaged with IPOL. However, the image quality may be affected by the tissue scattering and shallow depth-of-field. The chordae selected was thin enough to produce good results without sectioning. Other tissues worked better sectioned. Thicker chordae or other

tissues may require sectioning if their scattering is strong or if their microarchitecture is complex. A thin section may have a substantial effect on the biomechanics of the structure under study. It is essential to carefully consider this when deciding to use IPOL or interpreting results obtained from it. IPOL shares this limitation with other techniques based on transmitted light. However, because of the use of cumulative retardance, IPOL is particularly sensitive to sample thickness. In some conditions, such as thick samples, it may be more appropriate to use techniques based on reflected light, such as structured polarized light microscopy [45], second harmonic generated imaging [41]and confocal microscopy [46], or full-thickness techniques, such as small angle light scattering [42]. Similar to other light microscopy techniques, if a sample is larger than the field-of-view of a specific microscope configuration, image mosaicking is needed to acquire the entire view of the sample. Image mosaicking in IPOL would be most appropriate for imaging samples that are still, or moving slowly, rather than imaging tissue dynamics. For briefness, in this work we demonstrated IPOL using only one sample of each tissue. In our laboratory we have obtained reliable and repeatable results for tissues from several species, including sheep, pig, rat, guinea pig, monkey and human. Nevertheless, further work is necessary to establish if the measurements are affected by differences between species or samples, for example in collagen type.

5 | CONCLUSIONS

In this study, we present IPOL as a technique for imaging connective tissues with high spatial and temporal resolutions. IPOL optically encodes collagen orientation and architecture information in a single snapshot image with color and intensity, respectively, without post-processing. The real-time imaging capability of IPOL allows to quantify changes in collagen morphology and architecture under dynamic loading, which can provide valuable information for the understanding of tissue dynamics.

CONFLICT OF INTEREST
Bryn Brazile was at the University of Pittsburgh when he contributed to this work. He is now at Baxter.

DATA AVAILABILITY STATEMENT
The data that support the findings of this study are available from the corresponding author upon reasonable request.

ORCID
Ian A. Sigal https://orcid.org/0000-0002-0790-7911

REFERENCES
[1] B. Yang, J. Lesicko, M. Sharma, M. Hill, M. S. Sacks, J. W. Tunnell, *Biomed. Opt. Express* **2015**, *6*, 1520.
[2] P. Fratzl, *Collagen*, Springer, Boston, MA, **2008**, p. 1.
[3] J. E. Bischoff, E. M. Arruda, K. Grosh, *J. Biomech.* **2000**, *33*, 645.
[4] M. J. Girard, A. Dahlmann-Noor, S. Rayapureddi, J. A. Bechara, B. M. Bertin, H. Jones, J. Albon, P. T. Khaw, C. R. Ethier, *Invest. Opthalmol. Vis. Sci.* **2011**, *52*, 9684.
[5] N.-J. Jan, K. Lathrop, I. A. Sigal, *Invest. Opthalmol. Vis. Sci.* **2017**, *58*, 735.
[6] C. Boote, I. A. Sigal, R. Grytz, Y. Hua, T. D. Nguyen, M. J. Girard, *Prog. Retinal Eye Res.* **2019**, *74*, 100773.
[7] M. S. Sacks, A. P. Yoganathan, *Philos. Trans. R. Soc. Lond. B Biol. Sci.* **2007**, *362*, 1369.
[8] N.-J. Jan, J. L. Grimm, H. Tran, K. L. Lathrop, G. Wollstein, R. A. Bilonick, H. Ishikawa, L. Kagemann, J. S. Schuman, I. A. Sigal, *Biomed. Opt. Express* **2015**, *6*, 4705.
[9] W. Goth, S. Potter, A. C. Allen, J. Zoldan, M. S. Sacks, J. W. Tunnell, *Ann. Biomed. Eng.* **2019**, *47*, 1250.
[10] E. Götzinger, M. Pircher, M. Sticker, A. F. Fercher, C. K. Hitzenberger, *J. Biomed. Opt.* **2004**, *9*, 94.
[11] M. Shribak, R. Oldenbourg, *Appl. Opt.* **2003**, *42*, 3009.
[12] V. Gruev, R. Perkins, T. York, *Opt. Express* **2010**, *18*, 19087.
[13] T. York, S. B. Powell, S. Gao, L. Kahan, T. Charanya, D. Saha, N. W. Roberts, T. W. Cronin, J. Marshall, S. Achilefu, *Proc. IEEE* **2014**, *102*, 1450.
[14] S. Bancelin, A. Nazac, B. H. Ibrahim, P. Dokládal, E. Decencière, B. Teig, H. Haddad, H. Fernandez, M.-C. Schanne-Klein, A. De Martino, *Opt. Express* **2014**, *22*, 22561.
[15] B. Yang, N. J. Jan, B. Brazile, A. Voorhees, K. L. Lathrop, I. A. Sigal, *J. Biophotonics* **2018**, *11*, e201700356.
[16] S. V. Jett, L. T. Hudson, R. Baumwart, B. N. Bohnstedt, A. Mir, H. M. Burkhart, G. A. Holzapfel, Y. Wu, C.-H. Lee, *Acta Biomater.* **2020**, *102*, 149.
[17] A. Keikhosravi, Y. Liu, C. Drifka, K. M. Woo, A. Verma, R. Oldenbourg, K. W. Eliceiri, *Biomed. Opt. Express* **2017**, *8*, 4243.
[18] X. Wu, M. Pankow, H.-Y. S. Huang, K. Peters, *J. Biomed. Opt.* **2018**, *23*, 116002.
[19] X. Wu, M. Pankow, H.-Y. S. Huang, K. Peters, *Meas. Sci. Technol.* **2017**, *29*, 015203.
[20] W. Kaminsky, E. Gunn, R. Sours, B. Kahr, *J. Microsc.* **2007**, *228*, 153.
[21] M. V. Smith, R. M. Castile, R. H. Brophy, A. Dewan, D. Bernholt, S. P. Lake, *Am. J. Sports Med.* **2019**, *47*, 151.
[22] T. York, L. Kahan, S. P. Lake, V. Gruev, *J. Biomed. Opt.* **2014**, *19*, 066011.
[23] M. Shribak, *Sci. Rep.* **2015**, *5*, 17340.
[24] B. Wang, Y. Hua, B. L. Brazile, B. Yang, I. A. Sigal, *Acta Biomater.* **2020**, *113*, 429.

[25] E. Collett, *Field guide to polarization*, Spie Bellingham, WA **2005**.

[26] C. Hurlbut Jr., J. L. Rosenfeld, *Am. Mineral.* **1952**, *37*, 158.

[27] J. Schanda, *Colorimetry: Understanding the CIE System*, John Wiley & Sons, Hoboken, NJ, **2007**.

[28] N. Ohta, A. Robertson, *Colorimetry: Fundamentals and Applications*, John Wiley & Sons, Hoboken, NJ, **2006**.

[29] T. A. Wren, S. A. Yerby, G. S. Beaupré, D. R. Carter, *Clin. Biomech.* **2001**, *16*, 245.

[30] J. Schindelin, I. Arganda-Carreras, E. Frise, V. Kaynig, M. Longair, T. Pietzsch, S. Preibisch, C. Rueden, S. Saalfeld, B. Schmid, *Nat. Methods* **2012**, *9*, 676.

[31] I. A. Sigal, J. G. Flanagan, I. Tertinegg, C. R. Ethier, *Invest. Opthalmol. Vis. Sci.* **2004**, *45*, 4378.

[32] J. Ritchie, J. Jimenez, Z. He, M. S. Sacks, A. P. Yoganathan, *J. Biomech.* **2006**, *39*, 1129.

[33] T. W. Lin, L. Cardenas, L. J. Soslowsky, *J. Biomech.* **2004**, *37*, 865.

[34] A. P. Voorhees, N.-J. Jan, M. E. Austin, J. G. Flanagan, J. M. Sivak, R. A. Bilonick, I. A. Sigal, *Invest. Opthalmol. Vis. Sci.* **2017**, *58*, 5336.

[35] J. Lam, N. Ranganathan, E. Wigle, M. Silver, *Circulation* **1970**, *41*, 449.

[36] N.-J. Jan, C. Gomez, S. Moed, A. P. Voorhees, J. S. Schuman, R. A. Bilonick, I. A. Sigal, *Invest. Opthalmol. Vis. Sci.* **2017**, *58*, 3378.

[37] J. Wallace, N.-J. Jan, A. Gogola, M. Iasella, K. L. Lathrop, A. P. Voorhees, H. Tran, I. A. Sigal, *Invest. Opthalmol. Vis. Sci.* **2017**, *58*, 3162.

[38] A. Gogola, N.-J. Jan, K. L. Lathrop, I. A. Sigal, *Invest. Opthalmol. Vis. Sci.* **2018**, *59*, 4763.

[39] C. Millington-Sanders, A. Meir, L. Lawrence, C. Stolinski, *J. Anat.* **1998**, *192*, 573.

[40] N.-J. Jan, I. A. Sigal, *Acta Biomater.* **2018**, *72*, 295.

[41] S. Ram, F. Danford, S. Howerton, J. J. Rodríguez, J. P. V. Geest, *IEEE Trans. Biomed. Eng.* **2017**, *65*, 1617.

[42] M. S. Sacks, D. B. Smith, E. D. Hiester, *Ann. Biomed. Eng.* **1997**, *25*, 678.

[43] S. B. Mehta, M. Shribak, R. Oldenbourg, *J. Opt.* **2013**, *15*, 094007.

[44] M. Sivaguru, S. Durgam, R. Ambekar, D. Luedtke, G. Fried, A. Stewart, K. C. Toussaint, *Opt. Express* **2010**, *18*, 24983.

[45] B. Yang, B. Brazile, N.-J. Jan, Y. Hua, J. Wei, I. A. Sigal, *J. Biomed. Opt.* **2018**, *23*, 106001.

[46] I. Saytashev, S. Saha, J. Chue-Sang, P. Lopez, M. Laughrey, J. C. Ramella-Roman, *Opt. Lett.* **2020**, *45*, 2168.

SUPPORTING INFORMATION

Additional supporting information may be found online in the Supporting Information section at the end of this article.